Development of a 3D printed micro simulated moving bed chromatography system

Juliane Diehm, Tim Ballweg, Matthias Franzreb*

Institute of Functional Interfaces, Karlsruhe Institute of Technology, Eggenstein-Leopoldshafen 76344, Germany

ARTICLE INFO

2010 MSC:
00-01
99-00

Keywords:
Continuous chromatography
Microfluidics
µSMB
Continuous buffer exchange
Process miniaturization

ABSTRACT

In the 1960s, chromatography processes were revolutionized by the invention of simulated moving bed chromatography. This method not only enhances the separation performance and resin utilization in comparison to batch-chromatography, it has also a much lower buffer consumption. While simulated moving bed chromatography nowadays is applied for a wide range of industrial applications, it was never transferred to the micro-scale (in regards to column and system volume). In our opinion a micro simulated moving bed chromatography system (µSMB) would be a useful tool for many applications, ranging from early process development and long term studies to downstream processing of speciality products. We implemented such a µSMB with a 3D printed central rotary valve and a microfluidic flow controller as flow source. We tested the system with a four zone open loop setup for the separation of bovine serum albumin and ammonium sulfate with size exclusion chromatography. We used four process points and could achieve desalting levels of BSA ranging from 94% to 99%, with yields ranging form 65% to 88%. Thus, we were able to achieve comparable results to common lab scale processes. With a total dead volume of 358 µL, including all sensors, connections and the valve, this is, to the best of our knowledge, the smallest SMB system that was ever built and we were able to perform experiments with feed flow rates reaching as low as 15 µL/min.

1. Introduction

Continuous manufacturing is of rapidly increasing importance to the biopharmaceutical industry as more product can be produced in less time and at lower costs compared to batch processes [1–3]. Within biopharmaceutical down-stream processing, chromatography is one of the most frequently applied unit operations and hence special attention is paid to this step [1,4]. Simulated moving bed chromatography (SMB) is a frequently considered continuous implementation of chromatography [4,5]. It combines the common advantages of continuous processes, like higher productivity and consistent product quality [3,4,6], with the high efficiency and selectivity of a counter current operation, resulting in better resin utilization and lower buffer consumption in comparison with batch-chromatography [7,8]. Due to its numerous advantages, SMB has become a state of the art separation technique for many separation tasks in different industries, like the separation of *p*-xylene from other xylenes (Parex process) in the petrochemical industry [9], the separation of isomers in the sugar industry [10], or the enantioseparation for fine chemicals and pharmaceuticals [11].

However, the advantages of the SMB principle come at a price; as a result of the greater number of design and process parameters, like number of columns per zone and the zone flow rates, the process development is more sophisticated [4]. This can be a challenge, especially for the biopharmaceutical industry, where only a limited amount of product is available at early development stages. To save product, processes are therefore usually scaled down during process development [12–14]. This approach is particularly beneficial for continuous processes, as they have higher throughput than batch processes and hence greater product amounts are required to perform one experiment, especially if the process should be run over a longer time frame in steady state. However, with current lab and pilot scale SMB devices this can only be done to a certain limit, as the instruments provide stable flow rates merely in the mL/min range and the dead volumes of the systems are too high to handle small volumes efficiently.

In our opinion, a further down scale to the µL/min range has the potential to save many resources during process development

* Corresponding author.
E-mail address: matthias.franzreb@kit.edu (M. Franzreb).

in terms of time, resin and sample, especially for long-term studies, e.g. to investigate resin reusability, cleaning protocols or process stability. Thus, we decided to develop a micro SMB (µSMB) system which allows both the downscaling of the flow rates and the column volumes into the µL range. At the same time, we aim to maintain the benefits of current lab scale systems, like the easy adaptability to various process variants and the adjustment of the number of columns in a short time frame as well as the option to use the system as a disposable device.

In 2006, Subramini and Kurup showed in a theoretical study, that a downscale of the SMB principle to the µL-range in regard to column volume can separate a mixture of phenol and *o*-cresol with high yield and purity [15]. However, the study was completely theoretical and solely based on the separation performance of the columns. Important hardware considerations were not addressed and to the best of our knowledge, this theoretically study was never experimentally validated. Also some SMB equipment vendors already hold patents on so called *micro SMB systems*, but in this case the term *micro* seems to be used to distinguish from preparative SMB systems that are designed for product throughput of several tens of tons per year with column volumes in the m^3 range and not a reference to the actual scale of the system. The mentioned systems either have flow rates in the mL/min ballpark [16], or the used columns have a column volume of several mL [17]. These systems are comparable to the aforementioned lab, pilot or small scale systems [18,19]. Besides the commercially available systems, there are some self built SMB devices that work with lower flow rates, i.e. 200–900 µL/min, e.g. the HPLC-SMB of Pedeferri et al. [20] or the ÄKTA-SMB by Kröber et al. [21], but they still use columns with a column volume of several mL.

In this paper, we present our approach for the development of a µSMB system. First, we discuss our design considerations regarding the hardware wise implementation of the µSMB system, followed by a proof of concept study. Here, we used four process points for the desalting of the protein bovine serum albumin (BSA) from the salt ammonium sulfate (AS) by size exclusion chromatography (SEC)-SMB to showcase the functionality of the setup. Finally, we used process modelling and simulation to assess the performance of our system.

2. Design considerations

First we made a general assessment of the points that are critical for the downscale in order to maintain the SMB functionality. We won't give a detailed description of the SMB principle here, for this we refer to the extensive literature, e.g. [11,22–24]. Examples for SEC-SMB processes can be found in [25–27].

In a classical SMB setup, the binary separation of two components is achieved in zones two and three by adjusting the mean residence time in the respective zone between the retention times of both components [23]. This is achieved by cyclic switching of the columns in combination with setting different flow rates in the SMB zones. Hence, the generation of precise, fluctuation- and pulsation-free flow in each of the SMB zones is essential for the functionality. The flow rate deviation of many commercial lab scale systems is specified as ± 2% with a working range in the mL/min scale [28,29]. This results in absolute flow rate deviations in the ± 100 µL/min scale, which is within or even above the working range of a potential µSMB system. The lab scale systems usually use piston pumps as flow source, however, they are not suitable for the miniaturization of chromatography systems, as they are comparably large and prone to pressure pulsations [30]. In the field of microfluidics, other pressure sources, like electroosmotic pumps [31] or pressure driven microfluidic flow controllers [32,33] are more commonly applied [30]. We decided to use a pressure driven microfluidic flow controller in combination with a closed-loop flow rate control, as this system is ideal for the parallel generation of multiple flows in the µL/min range [34].

Even more important than the zone flow rates are the separation performances of the respective zones. Besides the chromatography columns itself, the system volume (also referred to as dead volume) can have a major influence on the system's separation performance [35]. The effect of dead volume on SMB processes has been extensively studied: Generally, the dead volume should be kept as low as possible, especially if high purities are required [36]. Particularly components that induce mixing effects, like check valves and pumps have a huge impact on the separation efficiency and should therefore not be placed between the columns [37]. Hence, we decided to implement the µSMB as an open-loop setup; this way it is not necessary to place a recycle pump between zones one and four. The diluent can still be recycled offline if required, e.g. by cyclical switching of waste and diluent reservoir [20].

The remaining contributions of the capillary dead volume (tubing and valve) can be divided into two portions:

(1) It causes a time delay, as the components need time to travel through the dead volume. This can be accounted for during the determination of the process point, e.g. by adapting the species retention times or by increasing the switching time [37]. Under the assumption that the dead volume is symmetrically distributed throughout all zones, this does not present a limitation for the downscale [38].

(2) It induces peak broadening while the species passes through the dead volume. This effect can decrease the separation performance of the system and thus should be considered [37]. Here, the dead volume between the chromatography columns is of particular importance [35], as it has a direct influence on the respective zone's resolution. Usually, the chosen valve system has the greatest impact on the system's inter-column dead volume, not only due to its own volume, but also because it determines the connection scheme [39]. The first SMB systems featured one central rotary valve but nowadays common commercial lab-scale systems as well as the aforementioned custom SMB systems use valve systems consisting of either several multiport or 2-way-valves [39]. These systems have the advantage that they can easily be adapted to a varying number of columns and that they can be used in various configurations, as the ports can be switched independently. This way, numerous processes can be realized on one system, which is especially useful in process development. On the other hand, these systems have the disadvantage that the connection scheme with the multiple valves requires lots of tubings which results in a higher dead volume compared to systems with a rotary central valve [39]. Hence, we decided to use the the original approach with one central rotary valve.

Besides the lower flexibility, typically mentioned disadvantages of this approach are that the systems are prone for cross-contamination and leakage. The cross-contamination results from commonly used channels for multiple streams that are necessary to connect all streams with all columns when both in- and outlet streams and columns are connected to the valve's stator. Both disadvantages have less impact in case of a µSMB: As the columns are smaller, they can be connected and turned with the valve's rotor. This enables a connection scheme without cross-over-channels, reducing the risk of cross-contamination. In addition, the whole valve is much smaller which makes the sealing of the system much easier. The reduced flexibility of rotary valves can be overcome by using 3D printing for the manufacturing of the valve system. This way, it can be easily adapted and manufactured in the time frame of one day in order to change the system to another process or a different number of columns. In the following sections, a detailed description of the system is given.

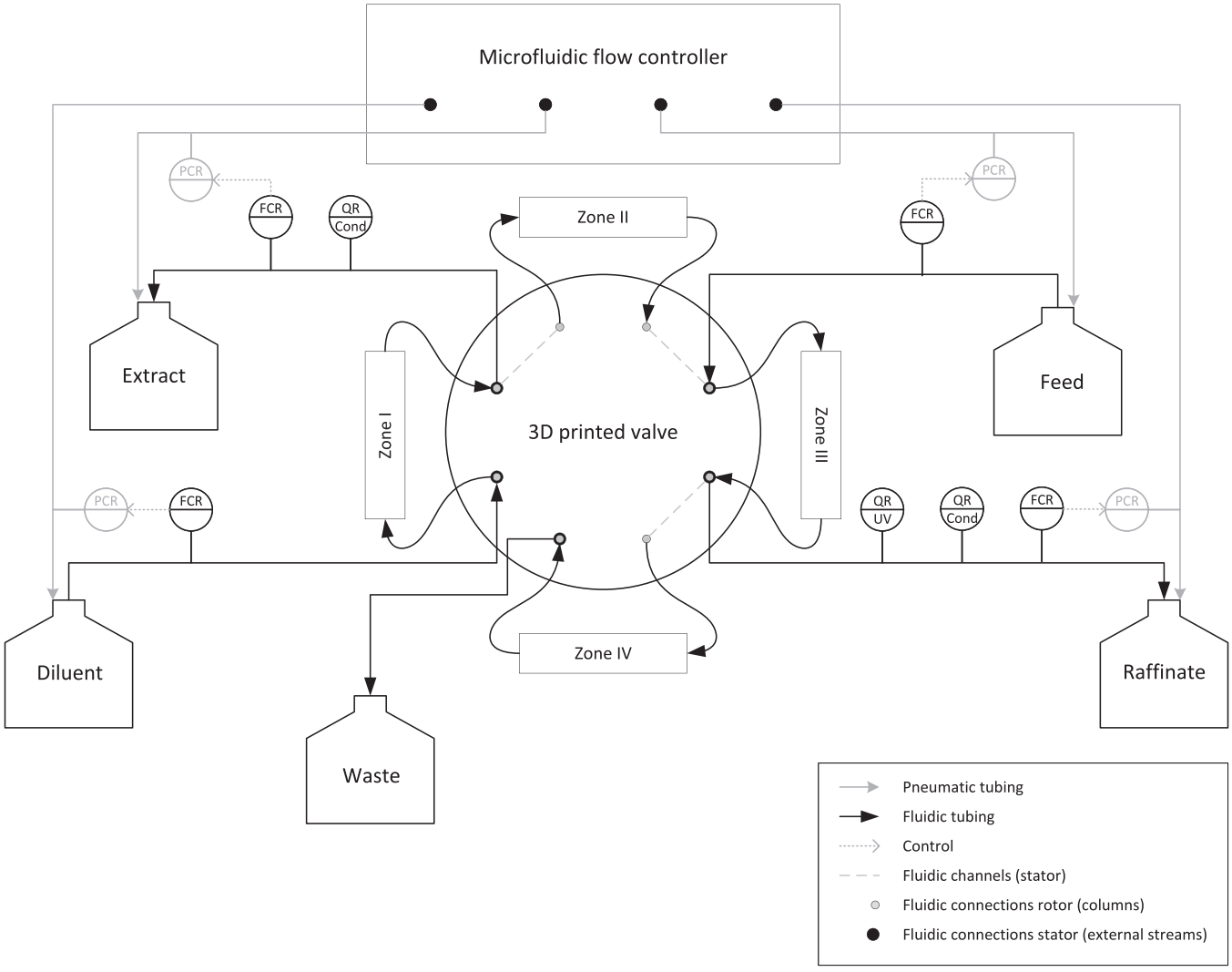

Fig. 1. Instrumentation and piping diagramm of the used SMB setup, *FCR: Flow–Control–Record; PCR: Pressure–Control–Record; QR: Quality–Record.*

3. Materials and methods

3.1. Experimental setup

In this section, the general setup of the µSMB is explained. In addition, further details about the flow control and the used chromatography columns are given.

3.1.1. General setup

The proposed µSMB system is a four zone open-loop setup with one column per zone. Figure 1 shows an instrument and piping diagram of the system. The experimental setup is depicted in Fig. 2. The SMB functionality is realized with a 3D printed central rotary valve, whose manufacturing process and characterization has been described in [40]. The rotary valve was implemented as a two disk design, where the columns are connected and moved with the valve's rotor, as this is in the case of miniaturization particularly promising [19]. The valve's stator contains channels to connect the chromatography columns as well as for the addition and withdrawal of external streams. On the rotor, the ports connecting the chromatography columns are organized in two concentric circles, one for the column-inlet-ports and one for the column-outlet-ports. All ports form a rectangle. This way the distance between the ports is minimized. Furthermore, the cross-contamination risk between the in- and outlets is reduced, as they follow different trajectories (for an illustration of the difference of this approach and one where all ports are placed on one circle, see also Figure S1 in the supplementary information (SI)). The chromatogra-

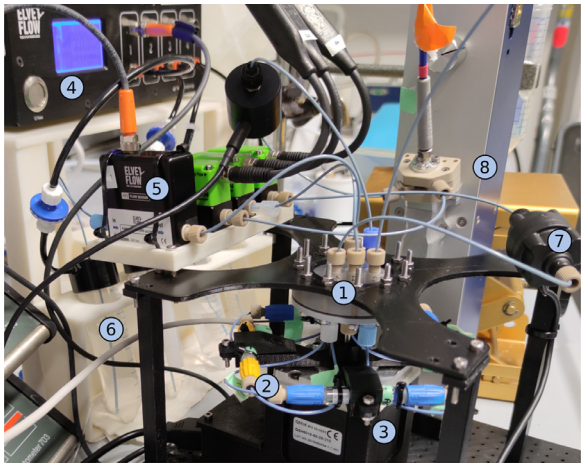

Fig. 2. The µSMB system: 1: 3D printed rotary valve; 2: chromatography columns connected to the valve's rotor and the motor shaft; 3: motor; 4: microfluidic flow controller; 5: flow sensors; 6: liquid reservoirs; 7: conductivity sensor; 8: UV sensor.

phy columns are aligned in a horizontal rectangle and connected to the rotor and the motor shaft with a 3D printed adapter. This layout allows for an efficient connection of the columns to the valve. The valve is turned with a stepper motor (pan drive PD60-3-1161, TRINAMIC Motion Control GmbH & Co. KG, Hamburg, DE); a short clip showing the switching process is included in the SI. The system flow is generated with a microfluidic flow control system (OB1 M3K+, Elveflow, an Elvesys brand, Paris, FR) in combination with flow sensors (SLI-1000, Sensirion AG, Stäfa, CF) in diluent, extract, feed and raffinate streams. The applicable flow rate range is defined by the measuring range of the flow sensors (here: 15–1000 µL/min) and the maximum pressure of the microfluidic flow controller (here: 6 bar) and can be adapted (if required) by choosing different hardware. The system is also equipped with conductivity sensors (ÄKTApurifier, Cytiva Life Sciences, Uppsala, SE) with conductivity meters (Labor-Konduktometer 703, Knick Elektronische Messgeräte GmbH & Co. KG, Berlin, DE) in extract and raffinate stream and a UV sensor (Qmax V, Cetoni GmbH, Korbussen, DE) in the raffinate stream for process control and evaluation. The 3D printed valve has an internal volume of 46.7 µL, the volume of the tubing that is used to connect the columns to the valve is 43.2 µL and the system has a total volume (excluding chromatography columns) of 358.1 µL. Considering the used sensors, the flow sensors have the greatest contribution to the dead volume with 25 µL each. With a total column volume of 1412 µL, this corresponds to a ratio of dead volume to system volume of 25.4% for the whole system and of 6.4% for the part relevant for the separation, which consists of the valve and the capillaries connecting valve and columns. The dead volume of preparative SMB systems is usually in the range of 3% of the column volume [36]. For small scale systems, the percentage can be much higher; Gomes et al. reported 11% for their FlexSMB unit [38], and there are even some reports where the system and the column volume were in the same order of magnitude [20,37]. However, Minceva et al. observed a significant loss of an SMB system's performance with increases in dead volume as small as 1% [35].

3.1.2. Flow control

As mentioned above, a microfluidic flow controller was used as flow source. This device works by pressurizing a vessel and thereby forcing the liquid out. Thus, an accurate and pulsation free flow is generated, even in the lower µL/min range [41]. In contrast to piston pumps this presents not a volume but a pressure driven pumping approach. The pressure in a chromatography system can vary over one process, for example due to viscosity changes in the mobile phase during sample loading [42], thus a closed-loop controller is necessary for a pressure driven approach in order to keep the flow rate constant. A time-discrete PI-controller according to (1) was implemented for this purpose, where p_t is the current set pressure, p_{t-1} is the set pressure of the previous time step, $P_{C,t}$ is the proportional term that is calculated with the difference of the set (Q_{set}) and actual flow rate ($Q_{actual,t}$) for each time step according to (2) and $I_{C,t}$ is the integration term, which is the sum overall $P_{C,t}$ values of all time steps as shown in (3).

$$p_t = p_{t-1} + k_p P_{C,t} + k_i I_{C,t} \tag{1}$$

$$P_{C,t} = Q_{set} - Q_{actual,t} \tag{2}$$

$$I_{C,t} = \sum_{t=0}^{t} P_{C,t} \tag{3}$$

The parameters k_p and k_i were determined with the method of Ziegler-Nichols [43] with a single chromatography column as controlled system. After fine tuning, k_p was set to 0.8 and k_i to 0.009, respectively. The control rate was set to 300 ms. In the µSMB setup the flow rates of four streams are controlled (diluent, feed, extract, raffinate), while the fifth flow rate (waste) is adjusted automatically due to mass balance. The flow rates and thus the flow control of the four streams are not independent of each other, as they form an interconnected system in the SMB; in the next step it was therefore tested if the single channel control could also be applied for the SMB setup. A stable flow for all streams could be generated with a feed-forward control. First start values were estimated with the Bernoulli equation [44] for the pressure drop in capillaries and the valve system and the Darcy equation [45] for the pressure drop in chromatography columns. Later on, the stationary pressures from a first test run were used as start values. To further stabilize the system flow, the controllers of the different streams were not started at once but staggered, starting with the diluent stream and going counterclockwise to the raffinate stream with a time delay of 100 ms between each stream.

3.1.3. Chromatography columns

Omnifit BenchMark Microbore chromatography columns (3x50 mm, column volume approx. 353 µL, Diba Industries Inc., Danbury, US) with stainless steel end pieces were used as column housings. The columns were packed with Sephadex G-25 Fine buffer exchange medium (Cytiva Life Sciences, Uppsala, SE), which has a particle size in the range from 20 µm to 80 µm in the dry and from 33 µm to 140 µm in the wet state. The slurry was prepared according to the manufacture's specifications and columns were packed using a pack adapter and deionized water as mobile phase. The column was connected to an ÄKTApurifier (Cytiva Life Sciences, Uppsala, SE) controlled with UNICORN 5.2 and the bed was compressed by increasing flow rates from 0.1 mL/min to 0.5 mL/min with a step increment of 0.1 mL/min. Each step was held for at least 10 min. Afterwards the pack adapter was removed and the column was washed for another 40 min at a flow rate of 0.3 mL/min with deionized water. In total four columns were packed.

3.1.4. Single column experiments

Single column experiments were performed to determine the column porosities and the retention times of BSA and AS. The experiments were conducted with an ÄKTApurifier at a flow rate of 0.3 mL/min with deionized water as mobile phase. For the determination of total and bed porosity, 2.5 µL of 1% (v/v) aceton or 1 g/L blue dextran solution, respectively, were injected. For the determination of the retention times of BSA and AS, 10 µL of a solution containing 1 g/L BSA (Sigma Aldrich, St. Louis, US) and 200 mM AS (Merck KGaA, Darmstadt, DE) were injected. All experiments were performed in triplicates for all columns. The hold-up volume of the system was determined by conducting the injections with a zero dead volume connector in place of a chromatography column. The porosities and retention times were calculated for all experiments and the mean value was used for process design.

3.1.5. SMB experiments

The feed solution for all SMB experiments contained 2 g/L BSA and 200 mM AS. Deionized water was used as diluent. Falcontubes (V = 50 mL) were used as reservoirs and connected to the flow controller with an adapter (Elveflow, an Elvesys brand, Paris, FR). The reservoirs for extract and raffinate were both filled with 2.5 mL of deionized water in order to prevent backflow of air into the SMB system during the start-up process. The system was flushed with deionized water and the feed stream was primed up to the central valve before the experiment was started. In addition, all reservoirs were weighed with a precision balance (Adventurer AX224, Ohaus Corporation, Parsippany, US) in order to calculate the mass balance of the process later on. The control of the

flow rates, the switching of the valve by the motor and the data logging of the pressures, flow rates and conductivities was handled by a custom Matlab application (Matlab R2020b, Mathworks Inc., Natick, US) with a graphical user interface during the experiments. The data logging of the UV absorption at 280 nm was done with the Qmix Elements software (Cetoni GmbH, Korbussen, DE). The flow rate control was paused for 1 s during the valve switching process and all pressures were kept constant at the last values before switching. The integral of the set point deviation ($I_{C,t}$) was set to zero and the controller was restarted after every valve switching. After the experiment was finished, the reservoirs were weighed again and the concentrations of BSA and AS were determined with off-line UV measurements (EnSpire multiplate reader, PerkinElmer, Waltham, US) and conductivity measurements (WTW LF330 conductivity meter with WTW Tetra con 325, Xylem Analytics Germany Sales GmbH & Co. KG, WTW, Weilheim, DE), respectively. The SMB system was reequilibrated with deionized water and then flushed with 20% ethanol for storage.

Five performance parameters were specified to assess the process points: the yield Y, the desalting efficiency DE, the dilution DL, the buffer consumption BC, and the productivity P, as defined by the following equations:

$$Y = \frac{c_{BSA,R} \cdot V_R}{c_{BSA,F} \cdot V_F} \cdot 100\% \tag{4}$$

$$DE = 1 - \frac{c_{AS,R}}{c_{AS,F}} \cdot 100\% \tag{5}$$

$$DL = \frac{c_{BSA,R}}{c_{BSA,F}} \cdot 100\% \tag{6}$$

$$BC = \frac{V_D}{V_F} \tag{7}$$

$$P = \frac{V_F}{4CV \cdot t_{end}} \tag{8}$$

All parameters were calculated using the results of the off-line measurements, with the concentrations of AS (c_{AS}) and BSA (c_{BSA}) in the reservoirs of the respective streams at the end of the experiment, the total processed volumes of the respective streams (V), the column volume of a single column (CV) and the overall process time (t_{end}).

3.2. Determination of process points

A process point for the first assessment of the µSMB system was determined using the triangle theory, which is commonly applied in literature [11,23,46]. The triangle theory is based on an ideal chromatography model, meaning the process point is solely selected based on the retention times of the pure components and all peak broadening effects are neglected [11]. The Henry coefficient of the species i H_i was calculated based on the retention time $t_{r,i}$ according to (9), where t_0 is the retention time of a tracer that can penetrate all pores and ϵ_t is the total porosity [47].

$$H_i = \left(\frac{t_{r,i}}{t_0} - 1\right) \frac{\epsilon_t}{1 - \epsilon_t} \tag{9}$$

The Henry coefficients were then used to create the triangle plot (see Fig. 3). Note that in the case of SEC, the Henry coefficients are negative, as the retention times of the species are smaller compared to the tracer due to the partial exclusion from the pores of the stationary phase. In the triangle plot m_j stands for the ratio of mobile phase flow to simulated stationary phase flow in the respective zone j:

$$m_j = \frac{Q_j t_s - CV\epsilon_t}{CV(1 - \epsilon_t)} \tag{10}$$

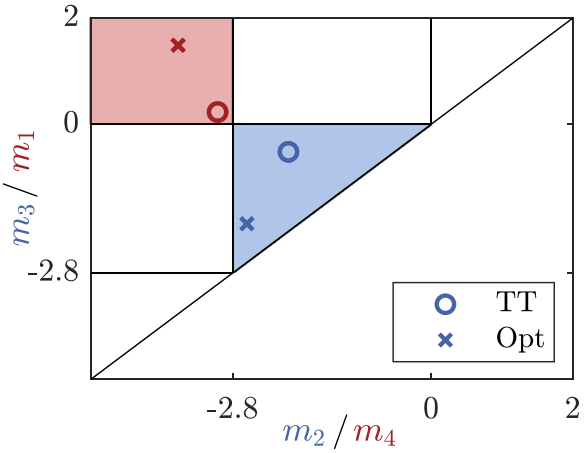

Fig. 3. Position of the process points in the m_2/m_3 and m_4/m_1 plane of the triangle plot. The area of complete separation in the m_2/m_3 plane is depicted in blue (triangle) and the area of complete regeneration of mobile and stationary phase in the m_4/m_1 plane is depicted in red (rectangle).

with the flow rate of the mobile phase Q_j, the switching time t_s and the column volume CV[37]. For the m_2/m_3 values, a point in the blue triangle of complete separation was chosen, for the m_4/m_1 values a point of complete regeneration of mobile and stationary phase close to the point of lowest buffer consumption was selected in the red rectangle. The feed flow rate was set to 30 µL/min. With these specifications, the remaining flow rates and the switching time were calculated with (10) and the five node balances of the open-loop SMB process ((11)–(15)).

$$Q_D = Q_1 \tag{11}$$

$$Q_E = Q_1 - Q_2 \tag{12}$$

$$Q_F = Q_3 - Q_2 \tag{13}$$

$$Q_R = Q_3 - Q_4 \tag{14}$$

$$Q_W = Q_4 \tag{15}$$

The determined flow rates and the switching time are given in Table 1. Experiments were also performed with halved flow rates and doubled switching time (0.5xTT) and doubled flow rates and halved switching time (2xTT), to show the robustness of the system. These process points all relate to the same positions in the triangle plot and thus should lead to the same results for an ideal process. To account for non-idealities, a process point was also determined using the general rate model (see row “Optimized” in Table 1). For this, the modeling and optimization tool CADET-SMB was used [48,49]. Details on the modeling process are given in the next section. The position of this process point in the m_1/m_4 and the m_2/m_3 plane is also depicted in Fig. 3.

3.3. Process modeling

The SMB processes at the respective process points were modeled using CADET-SMB (version 2.12) with CADET (version 3.2.1), in order to obtain comparative values for the experimental performance. Matlab Version R2020b was used for all simulations. A detailed description of the model procedure is given in the following sections. In addition, a tabular overview of all model input parameters is given in Table S1 in the SI.

Table 1
Overview of tested process points.

Process Point	Q_D in µL/min	Q_E in µL/min	Q_F in µL/min	Q_R in µL/min	t_s in s
Triangle Theory (TT)	113	45	30	50	165
Optimized (opt)	285	169	30	70	80
2xTT	226	90	60	100	82.5
0.5xTT	56.5	22.5	15	25	330

3.3.1. Single column modeling

As a first step, model parameters of a single column experiment were determined. For this the data of the single column experiments with BSA and AS described in Section 3.1.4 were used. In addition, the experiments were repeated at different flow rates (0.05 mL/min, 0.1 mL/min, 0.2 mL/min, 0.3 mL/min) to obtain the influence of the flow rate on the axial dispersion coefficient.

A series of continuous stirred tank reactors (CSTRs) was implemented into the single column model (see SI Figure S2) to account for the peak broadening effects of the Äkta system. The general rate model was chosen as chromatography model. The mass balances for the mobile and stationary phase are given in the SI, further details on the model equations and solver can be found in [50,51] and the CADET documentation [52]. The porosities were calculated based on the retention times of the tracer molecules. The pore accessibility (F) was determined with the retention times of BSA and AS. The mass transfer parameters axial dispersion (D_{ax}), film transfer coefficient (k_{film}) and pore diffusion coefficient (D_p) were estimated by adjusting the modelled chromatogram to the experimental one. D_p was set to zero for BSA, as it cannot penetrate the particle pores. The optimization was done with the genetic algorithm of the global optimization toolbox of Matlab. The population size was set to 100 with a maximum of 500 generations. The optimization parameters were the difference in simulated and experimental peak area (A), the difference in retention time (t_r) and the difference in peak height (h). The objective function was defined as follows:

$$y = k_A|A_{sim} - A_{\text{exp}}| + k_r|t_{r,sim} - t_{r,\text{exp}}| + k_h|h_{sim} - h_{\text{exp}}| \tag{16}$$

The penalty factors were set to $k_A = 1$, $k_r = 2$ and $k_h = 10$. First, the optimization was performed separately for BSA and AS. As it is only possible to enter the same D_{ax} for both components in CADET-SMB, the average of the determined D_{ax} of both components was calculated and used as a set value. A second optimization was performed to refine k_{film} for BSA and k_{film} and D_p for AS. D_{ax} was determined for all four flow rates, k_{film} and D_p were treated as independent of the flow rate.

3.3.2. SMB Modeling

CADET-SMB (version 2.1.2) was used for the simulation and optimization of the SMB process. The script was adapted to a four zone open-loop system. A simulation was performed for all process points given in Table 1. For comparison with the experimental mass balance, the simulated trajectories of both components in the different streams were integrated for the duration of the respective experiment. In addition, the integral over one cycle in cyclic steady state was calculated. The build in script of CADET-SMB using the differential evolution algorithm with a population size of 50 and a maximum number of generations of 200 was applied for the process point optimization. The aim of the optimization was to maximize purity of BSA in the raffinate stream. Thus, the objective function was defined to maximize yield of BSA in the raffinate ($Y_{BSA,R}$) and minimize yield of AS in the raffinate ($Y_{AS,R}$) at the same time:

$$y = k_{AS}Y_{AS,R} + k_{BSA}(Y_{BSA,R,\text{min}} - Y_{BSA,R}) \tag{17}$$

Table 2
Model parameters for the simulation of the separation of BSA and AS with the used columns. Values marked with * were directly calculated from the chromatograms, values marked with + are comparative values that were calculated with empirical correlations from literature. All other values were obtained from parameter fitting.

	BSA	AS
F^*	0 (1.0×10^{-5})	1
ϵ_t^*	0.844	
ϵ_p^*	0.743	
ϵ_{int}^*	0.394	
D_{ax} in m²/s	$5.21 \times 10^{-6} \cdot Q$ [mL/min]	
	5.21×10^{-7} (@ 0.1 mL/min)	
D_{ax}^+ in m²/s	1.17×10^{-7} (@ 0.1 mL/min)	
k_{film} in m/s	1.14×10^{-5}	3.00×10^{-6}
k_{film}^+ in m/s	1.75×10^{-5}	1.46×10^{-4}
D_p in m²/s	–	2.31×10^{-10}
D_p^+ in m²/s	–	2.30×10^{-10}

The penalty factors k_{BSA} and k_{AS} were set to 1 and 10, respectively. The required yield of BSA in the raffinate ($Y_{BSA,\text{min}}$) was set to 0.99.

4. Results and discussion

4.1. Model parameter estimation

The parameters that were determined for the simulation of the single column experiment are given in Table 2. The pore accessibility F and the porosities were calculated with the retention times of the components and the tracers, respectively. BSA is excluded from all pores, nonetheless for the simulations a value of 1.0×10^{-5} was used for the pore accessibility, since it can't be zero for mathematical determinacy. In contrast to that, AS is able to access the whole pore volume. In addition to the determined values for the mass transfer parameters, Table 2 shows the values calculated with empirical correlations. D_{ax} was calculated with the correlation of Chung and Wen [53], k_{film} was derived from the correlation by Wilson and Geankoplis [54] and D_p was calculated according to Satterfield et al. [55]. All experimentally determined parameters, except for the film transfer coefficient of AS, are in the same order of magnitude as the values predicted by the empirical correlations and thus are considered to be reasonable. The film transfer coefficient of AS is two orders of magnitude smaller compared to the correlation and it is even lower than the one of BSA. This is unlikely, as BSA has a higher molecular mass and therefore a lower diffusion coefficient. From the chromatogram in Fig. 4 it is clearly visible that the second peak, which is detected by the conductivity measurement and hence caused by AS is much broader than the first peak, which is visible in the UV signal and thus represents BSA. Most likely another effect is lumped into the value of k_{film} in order to account for this peak broadening. This could for example be caused by the longer residence time or the tortuosity of the pore system of the beads. Even though this value does not represent the physical value of AS's film transfer coefficient, the simulation is nonetheless able to reflect the experimental results, as it is shown exemplary for a flow rate of 0.3 mL/min in Fig. 4. Both, the retention time and the peak height are predicted precisely. There

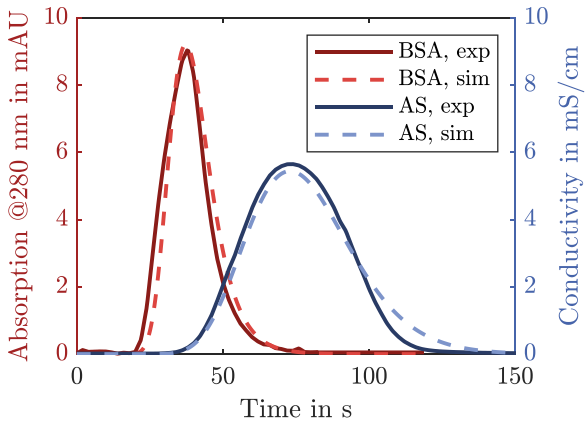

Fig. 4. Comparison of simulation and experimental results for the separation of bovine serum albumin (BSA) and ammonium sulfate (AS) with a single column at a flow rate of 0.3 mL/min.

are deviations at the slopes, particularly at the descending slope of AS; nonetheless, the fit quality is sufficient to calculate comparative values for the SMB experiments. Figure 4 also shows that there is no baseline separation of BSA and AS; however, there are regions of pure BSA and pure AS, which is usually sufficient for a separation with SMB [37].

4.2. Flow rate accuracy

The precise generation of flow rates in the µL/min range was identified as one of the critical factors for the successful implementation of a µSMB device. Thus, the flow rates were monitored and analyzed for the triangle theory process point. Figure 5a shows the flow rates of the four controlled in- and outlet streams for the first three cycles of the experiment in duplicates. The inlet streams are shown with positive flow rates and the outlet streams with negative ones. The first four valve switches are indicated with vertical gray lines. The results of both experiments are in good accordance with the set values, however short fluctuations are occurring during the switching process. This is because the back pressure of the system changes during the switching and in contrast to most other systems, the flow is not stopped. Similar pressure spikes during the switching process were also observed by Gomes et al. but they didn't report any negative effects [38].

Figure 5b depicts the pressures applied by the microfludic flow controller to generate the respective flows of Fig. 5a. The pressures follow a periodic pattern with the switching cycle, which indicates that the pressure drop differs for the four used chromatography columns. In addition, all pressures are higher for the second run, although the same columns were used. This illustrates that it is necessary to use a closed-loop control for the flow rates in this setup in order to account for the changes in pressure drop.

To assess the influence of the switching process on the overall flow rate accuracy, the mean flow rate recorded by the on-line sensors over the whole process was calculated. Additionally, off-line measurements were performed by weighing the reservoir vessels before and after the experiment. The results of the off- and on-line measurements are given in Fig. 5b. As there was no on-line measurement for the waste stream, only the off-line measurements are depicted. There is a slight discrepancy between the off- and on-line measurements but they are all (except the first off-line measurement of the feed stream) in the accuracy range of ±5% given by the flow sensor manufacturer. A different kind of flow sensor was used during the first experiment (TT1) in the feed stream. Here, the value is above 5%, but for the second run (TT2), where the sensor was changed to a SLI-1000 sensor, the accuracy is below 5% as

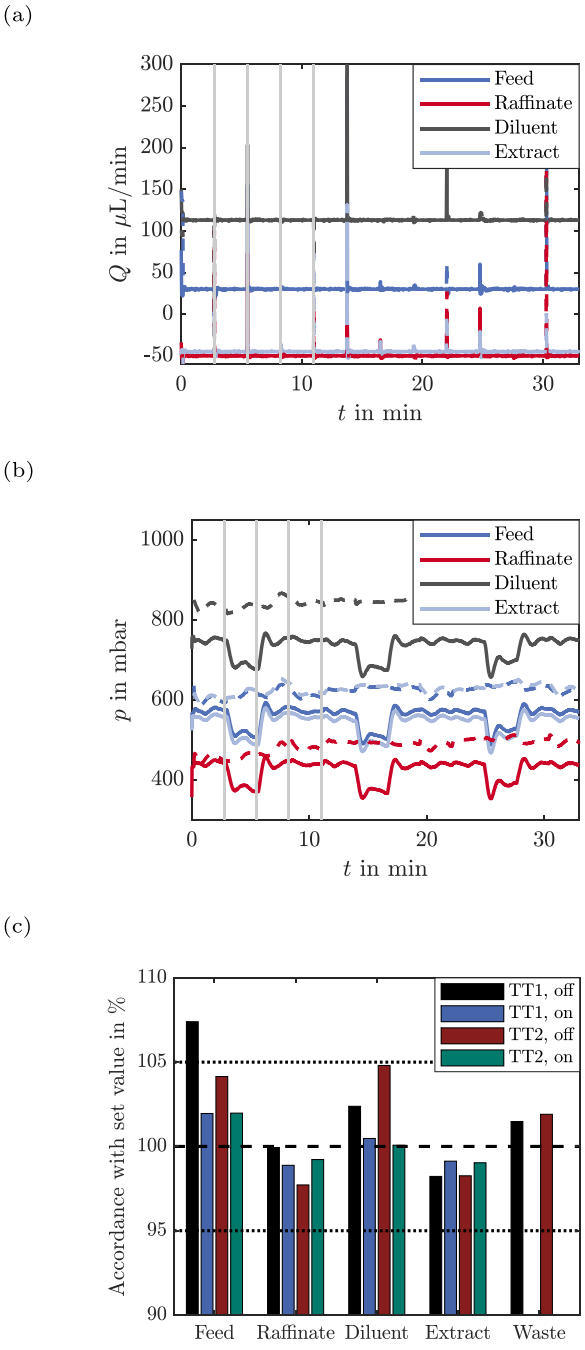

Fig. 5. Flow rate (a) and pressure curves (b) of the four controlled in- and outlet streams of the SMB system. Depicted are the first three cycles of both runs with the TT process point (TT 1: solid line, TT 2: dashed line). The first four switches are indicated with vertical gray lines. (c) Comparison of on-line and off-line flow measurements with the set value.

well. In most cases the deviation is even below ±2%. A difference between set and actual value is not only observed for the off-line, but also for the on-line measurements. This implies that there is a measurable influence of the switching process on the mean flow rate. Thus, the performance of the flow control could probably be further improved by fine tuning the PI controller for adaptions during the switching process. On the other hand, as described before, the fine tuning of this coupled system of controllers is not trivial. In addition, the flow rate accuracy of commercial systems is in the same range (e.g. BioSMB PD: ±5% [29], Octave 12 pump: ±2% [28]), even though the minimum flow rate is higher (e.g. BioSMB PD:

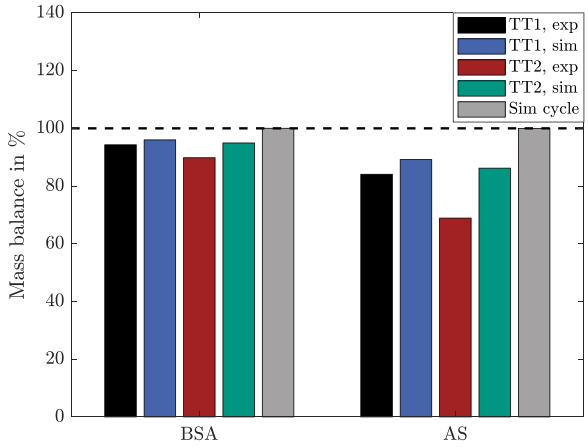

Fig. 6. Mass balance of BSA and AS for both TT runs in comparison to the simulation and the simulation of one process cycle in cylic steady state.

0.5 mL/min [29], Octave 12 pump: 0.2 mL/min [28]). Gomes et al. measured the fluctuation in the recycle stream of their system; the flow rate was in the range between 21 mL/min and 25 mL/min in the course of one cycle, which corresponds to fluctuations of ±8% [38]. Hence, the achieved flow rate accuracy of the µSMB system is acceptable for the conduction of SMB experiments.

4.3. Influence of dead volume

Besides the flow rate control, the dead volume is an important factor for the miniaturization of a SMB system. In the following the effects of the dead volume on the µSMB experiments will be assessed with the system's mass balance, trajectories and mean concentrations in the in- and outlet streams. The experimental results in this section are a duplicate run of the process point that was determined with the triangle theory (TT1 and TT2).

In order to assess the influence of the dead volume on the system's performance, process simulations were performed to obtain comparative values. The chromatography columns were modeled with the general rate model, thus the dispersion effects in the column were taken into account, but the dead volume and effects connected to it were not considered. This way, the simulated results represent an idealized system without any dead volume and the impact of the dead volume on the experiments can be estimated through comparison with the simulation.

4.3.1. Mass balance

Figure 6 shows the mass balances of BSA and AS for both runs. The experimental mass balance was calculated with the off-line concentration measurements. For comparison, the mass balance of the simulation is depicted. At first glance it is surprising that the mass balance does not reach 100% for the simulation. This is because the whole system is filled with water at the beginning of each experiment. After the experiment is stopped, part of the feed solution remains in the columns and other parts of the system, hence reducing the mass balance. This effect has less influence for longer process times, as the portion of feed solution remaining in the system compared to the overall amount of feed gets smaller. The mass balance predicted by the simulation differs for both runs since they were run for a different time: The process time of TT1 is 112 min, for TT2 it is only 88 min. The mass balance calculated with the simulation over one cycle in cyclic steady state (gray bars) is 100%. This shows that the mass conservation in the simulation is working.

In both experiments, AS has a lower recovery than BSA. This is caused by the broader peak width of AS (see Fig. 4), which causes AS to spread over the whole system in the course of the experiment. This is different for BSA, where the concentration remains at 0 g/L in some sections (compare the chromatograms in Fig. 7). This way more AS remains in the system when the experiment is stopped and thus the mass balance is reduced.

In addition, all experimental mass balances are lower than the simulated ones. This is due to the fact that the dead volume was not considered for the simulation but BSA and AS also remain in those parts of the system when the experiment is finished. For the reasons discussed before, this effect is larger for AS. The experimental mass balance of BSA only differs 2.8% and 5.4% from the simulation, indicating only a small influence of the dead volume. For AS these values are higher with 5.7% and 20.1%. However, these values would decrease for longer process times and the samples can be recovered by flushing the system after a run is finished. Thus, they do not represent a real loss.

4.3.2. Trajectories and chromatogram

The concentrations of BSA and AS at the raffinate and extract port were recorded on-line during the experiments with a sampling time of 1 s. The resulting trajectories of the first three cycles are depicted in Fig. 8 alongside the simulated results. Figure 8a shows the BSA concentration in the raffinate stream, Fig. 8b and c show the AS concentration in the raffinate and extract streams, respectively. The BSA concentration in the extract is not displayed, as no on-line measurement was performed. The switching times are indicated by the vertical gray lines in all figures.

The retention time was adjusted by the time delay caused by the dead volume between the valve system and the detectors for all measurements. In general, the results of both experimental runs are in good accordance with each other. This underlines the statement of the last paragraph, that the deviation in the mass balances is caused by the different lengths of the experiments and not by differences during the processes. All trajectories show a cyclic pattern with start up behavior, which is caused by the valve switchings and is typical for SMB processes.

The first peak of the experimental results of BSA is either missshaped or completely missing and all other peaks of the first cycle have a smaller peak area in comparison to the simulation. This behavior indicates that there is an interaction between BSA and some part of the SMB system. Most likely it is an interaction with the 3D printing material of the valve system, as this has been reported before [56]. After one cycle, BSA has been in contact with all parts of the 3D printed valve and the material is saturated, which results in a better prediction of the experimental peak shape by the simulation. After each valve switching, the BSA concentration drops abruptly. In the experiments the observed drop in concentration is neither as low nor as steep as predicted by the simulation. Additionally, the minimum BSA concentration is not reached right after the switching but slightly later. The latter effect is caused by the dead volume between valve and sensor. This part of the system (volume approx. 30 µL) is still filled with the solution leaving the previous column, thus there is a time delay until the effect of the switching process is measured. The remaining deviations result from peak broadening effects in the dead volume.

There is a breakthrough of AS into the raffinate stream at the end of each switching period in the experiment as well as the simulation, as it is shown in Fig. 8b. This was to be expected, as AS has a comparably high peak width in the single column experiment. Only the position of the peak maximum and not the peak width was considered during process point determination, thus leading to this impurity level. Comparing the simulation and experiments, it can be seen that the prediction of the retention time and height of the AS peaks is quite precise. In contrast to the simulation, the AS concentration does not drop to zero after each switching process in the experiments indicating peak broadening in the dead

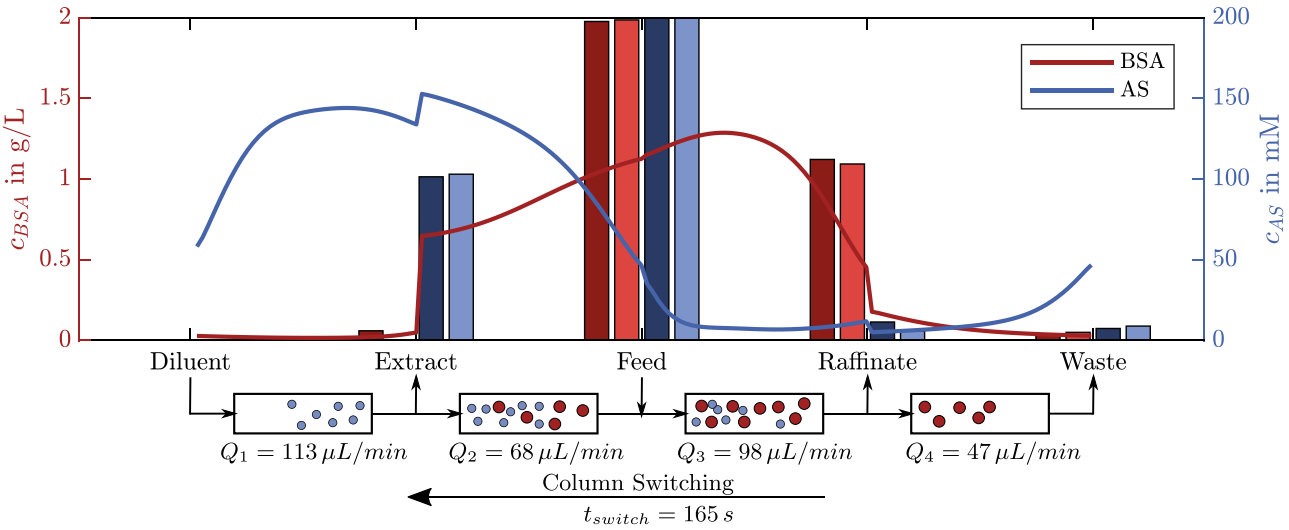

Fig. 7. Concentrations of BSA and AS in the reservoirs of the in- and outlet streams at the end of the TT1 experiment (dark colors) in comparison to the simulated concentrations (light colors). In addition, the simulated concentration profile right after switching in cyclic steady state in the zones as well as the zone flow rates are displayed.

volume. In this case, the not considered dead volume leads to an higher overall concentration of AS in the raffinate. When comparing the peak heights, it can be observed that each fourth peak is lower compared to the other ones. This indicates that one column differs from the other ones, which also explains the different back pressures observed in Fig. 5b.

Several observations can be made for the trajectory of AS in the extract: (1) At the beginning of the experiments, the AS concentration is lower than predicted; (2) the peak shape is different, particularly the concentration increase after switching is not as steep; (3) the peaks have a longer retention time compared to the simulation which is especially evident in the first cycle. The longer retention time is most likely caused by the time delay induced by the dead volume. This also leads to the differences in peak shape: The position were the AS peak is cut by the switching is close to the peak maximum in the simulation but not in the experiments. A possible explanation for the lower AS concentration is that the regeneration of the stationary phase in zone one is not sufficient and AS is transported from zone one into zone four with the stationary phase.

Comparing the simulated and experimental trajectories, deviations in retention time and peak height that are most likely caused by the dead volume are observable. However, it is difficult to determine how much this will effectively influence the process e.g. in terms of yield from the trajectories. Therefore, the measured (dark colors) and predicted (light colors) overall concentrations in the reservoirs after the experiment (TT1) are shown in Fig. 7. In addition, the chromatogram of the simulated concentrations in the zones at the beginning of a cycle in the cyclic steady state and the zone flow rates are depicted. The concentration of AS is always non-zero and it increases with the column length in the fourth zone. This indicates that the regeneration of the stationary phase in zone one is indeed not sufficient and as a consequence the diluent flow rate should be increased to improve BSA purity. In accordance with the trajectories, the experimental AS concentration is lower in the extract and higher in the raffinate compared to the simulation results. While the difference in the extract is less than 2%, the measured concentration in the raffinate is twice as high as expected. This comparably high relative error is partly due to the low concentration level itself. In regard to the feed concentration, the deviation is below 3%. The same is applicable for BSA. Thus, the observed overall deviation from the simulation and therefore the influence of the dead volume is small. It gets obvious from Fig. 7 that the µSMB system is capable to perform the separation of BSA from AS, even though the dead volume was not considered for the process design. To improve the purity of BSA as well as for the conceptualization of further studies, it still would be of interest to do additional investigations on the dead volume's effects. For example, from the shown results it cannot be determined if the time delay or the peak broadening have a greater influence on the process. In addition, it cannot be distinguished if band broadening occurs mostly in the volume between the valve and the detector, which only influences the peak shape but not the separation performance, or in the dead volume between the columns. This information would be important if the system was adapted for different kinds of processes as well as for the process transfer to other systems.

4.4. Performance of the process points

In the two previous sections, it was shown that the system meets the necessary requirements regarding flow rate control and dead volume. To conclude, the performance of the SMB system is evaluated by comparing the defined performance parameters of the process points. In addition to the aforementioned process point determined with the triangle theory, all flow rates were either halved (0.5xTT) or doubled (2xTT) to evaluate the system's behavior under different flow conditions. Furthermore, a process point was determined using the optimization function of CADET-SMB, with the aim of achieving the highest possible desalting efficiency (Table 1).

The results are depicted in Fig. 9, with Fig. 9a showing the experimental and Fig. 9b showing the comparative results of the respective simulation. In both figures, the results form the same pattern: 2xTT has the highest productivity, opt has the highest buffer consumption and the highest dilution, but it also has the highest desalting level and the lowest yield. In this case, the optimization algorithm traded off yield against purity.

In principle, the performance parameters can be divided into two groups. The productivity and the buffer consumption are determined by the chosen process point, while the yield, the desalting efficiency and the dilution depend on the separation performance. There are only slight differences between the experiments and simulations for the first group. They are caused by differences between the set and actual flow rates. As described before, this is

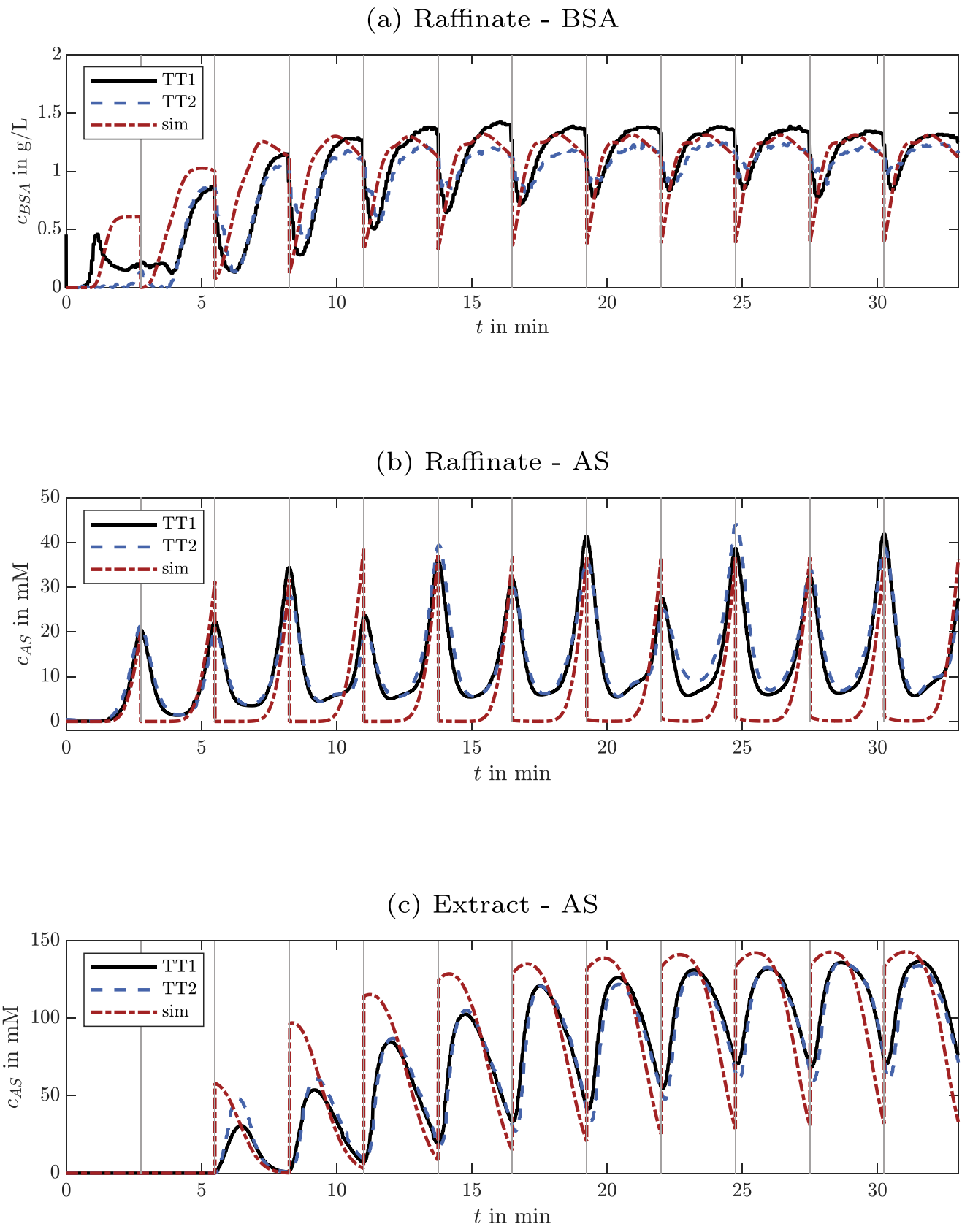

Fig. 8. Comparison of the experimental and simulated trajectories of the TT process point: (a): BSA trajectory in raffinate stream; (b) AS trajectory in raffinate stream (c) AS trajectory in extract stream.

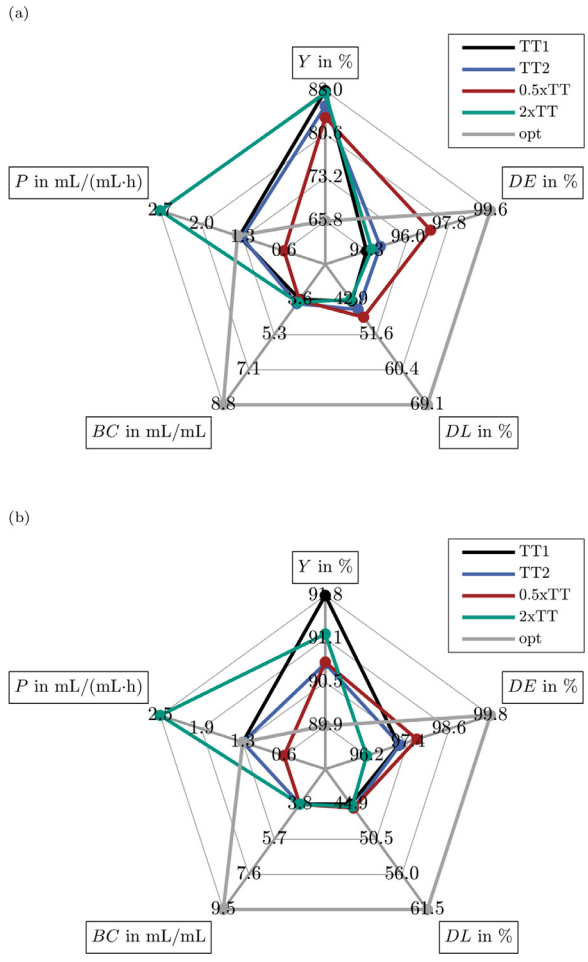

Fig. 9. Comparison of the performance parameters for the experiments (a) and the respective simulations (b). *Y*: yield; *DE*: desalting efficiency; *DL*: dilution; *BC*: buffer consumption; *P*: productivity.

due to disturbances during the switching process and the accuracy of the on-line flow sensors (see Section 4.2).

The experimental yield is lower as estimated with the simulation for all experiments. For most experiments, this deviation is in the range of 3–5% and can be explained by the portion of the BSA remaining in the dead volume of the system after the experiment is finished, as was discussed in the previous section (see Section 4.3). For the optimized process point, the difference is 24%, which can not be explained solely by this effect. Neither are the higher flow rates nor the shorter switching time the cause of this result, as they are comparable to 2xTT where this effect is not observable. Most likely the deviation is caused by the different ratios of the zone flow rates compared to the other experiments. The ratio of the highest to the lowest flow rate is much higher (3.8 vs 2.4), at the same time the ratio of the flow rates in zones three and two is a bit lower (1.26 vs 1.44). Due to the unconsidered inter-column dead volume, this causes more BSA to be transported in the direction of the extract port where it will be flushed out because of the high flow rate in zone one. In this case the yield can be improved e.g. by adapting the switching time.

In an ideal, dispersion free scenario, the results for TT, 0.5xTT and 2xTT should be identical. The simulation calculates identical values for the productivity and the buffer consumption; the differences in yield were discussed before. However, the desalting efficiency increases from 96.2% to 97.7% with decreasing flow rate. This is even more apparent for the experiments, where the results range from 94.2% to 97.0%. The reason for this observation is that in the flow rate range considered here, the axial dispersion is smaller for lower flow rates (see Table 2), thus there is less band broadening due to mass transfer limitations and less AS contaminates the raffinate. Consequently in this case, lower flow rates are favorable for the separation process. The optimization algorithm still chose higher flow rates for the optimized process point because dilution was not directly penalized in the objective function. From this point of view, the diluent flow rate should be infinitely high; however, a high diluent flow rate has a negative impact on the BSA yield and as this was considered in the objective function, the selected diluent flow rate is in a reasonable range.

In summary, all evaluated process points reached a desalting level above 94%, the optimized point even achieved a desalting efficiency of 99.6%. The yields were in the range from 85% to 88%, only the optimized point has a lower yield of 65.8%. These results are comparable to the ones reported by Hashimoto et al., who used comparable components with a larger setup [25]. This clearly shows that the µSMB system is capable of successfully performing separation processes under various conditions. An optimization under consideration of the dead volume could even increase the performance further in future works.

5. Conclusion

We were able to successfully develop a µSMB system. The main factors for downscale, flow rate accuracy and dead volume, were addressed with the use of a microfluidic flow controller and a 3D printed valve, respectively. The resulting ratio of inter-column dead volume to column volume is 6.4% for the developed system. As a proof of concept we tested the system for the separation of BSA and AS with SEC-SMB under different conditions. We were able to achieve desalting rates above 99%, reaching comparable levels to other systems [25]. Still, we saw some impact of the dead volume on the process, which should be further investigated in the future. The lowest applied feed flow rate was 15 µL/min, with the zone flow rates between 24 µL/min and 56.5 µL/min which is, to the best of our knowledge, the process with the lowest flow rates that was ever reported for a SMB experiment. The sample volume required to reach the cyclic steady state was as low as 3.3 mL.

The presented results thus provide the proof that SMB is not only a useful tool for preparative applications but can also be applied in a small scale, enabling a variety of new applications. For example, the µSMB system can be a useful tool in process development as a downscale model. For this, the comparability of the µSMB to common lab scale systems should be investigated as a next step. Furthermore, due to its low column volumes and low buffer and sample consumption, the system could be interesting for long term studies in regards to resin reusability or cleaning protocols. One big advantage of the presented system is that the main parts, the pump and the valve, are either not in contact with the product (pump) or can be manufactured at low costs in a short time (valve). This way the system is ideal as a disposable setup and can also be used for studies with toxic components without the possibility to cross-contaminate the next process. Additionally, because of its small footprint it can easily be placed in a common lab fume hood. The 3D printed valve system enables the easy adaption of the system to multiple processes but keeps the system simple at the same time, which makes it a perfect tool for research.

Declaration of Competing Interest

The authors declare that they have no known competing financial interests or personal relationships that could have appeared to influence the work reported in this paper.

CRediT authorship contribution statement

Juliane Diehm: Conceptualization, Methodology, Investigation, Software, Visualization, Writing – original draft. **Tim Ballweg:** Methodology, Investigation, Visualization, Writing – review & editing. **Matthias Franzreb:** Conceptualization, Writing – review & editing.

Acknowledgments

J.D. wants to thank the Cusanuswerk e.V. for the funding of her PhD scholarship.

References

[1] A. Jungbauer, Continuous downstream processing of biopharmaceuticals, Trends Biotechnol. 31 (8) (2013) 479–492, doi:10.1016/j.tibtech.2013.05.011.
[2] A.S. Rathore, H. Agarwal, A.K. Sharma, M. Pathak, S. Muthukumar, Continuous processing for production of biopharmaceuticals, Prep. Biochem. Biotechnol. 45 (8) (2015) 836–849, doi:10.1080/10826068.2014.985834. Publisher: Taylor & Francis
[3] F. Feidl, S. Vogg, M. Wolf, M. Podobnik, C. Ruggeri, N. Ulmer, R. Wälchli, J. Souquet, H. Broly, A. Butté, M. Morbidelli, Process-wide control and automation of an integrated continuous manufacturing platform for antibodies, Biotechnol. Bioeng. 117 (5) (2020) 1367–1380, doi:10.1002/bit.27296.
[4] L. Gerstweiler, J. Bi, A.P. Middelberg, Continuous downstream bioprocessing for intensified manufacture of biopharmaceuticals and antibodies, Chem. Eng. Sci. (2020), doi:10.1016/j.ces.2020.116272.
[5] A.C. Fisher, M.-H. Kamga, C. Agarabi, K. Brorson, S.L. Lee, S. Yoon, The current scientific and regulatory landscape in advancing integrated continuous biopharmaceutical manufacturing, Trends Biotechnol. 37 (3) (2019) 253–267, doi:10.1016/j.tibtech.2018.08.008.
[6] R.-M. Nicoud, The amazing ability of continuous chromatography to adapt to a moving environment, Ind. Eng. Chem. Res. 53 (10) (2014) 3755–3765, doi:10.1021/ie5005866.
[7] M. Wellhoefer, W. Sprinzl, R. Hahn, A. Jungbauer, Continuous processing of recombinant proteins: integration of refolding and purification using simulated moving bed size-exclusion chromatography with buffer recycling, J. Chromatogr. A 1337 (2014) 48–56, doi:10.1016/j.chroma.2014.02.016.
[8] J. Andersson, B. Mattiasson, Simulated moving bed technology with a simplified approach for protein purification: separation of lactoperoxidase and lactoferrin from whey protein concentrate, J. Chromatogr. A 1107 (1) (2006) 88–95, doi:10.1016/j.chroma.2005.12.018.
[9] M.S.P. Silva, A.E. Rodrigues, J.P.B. Mota, Modeling and simulation of an industrial-scale parex process, AIChE J. 61 (4) (2015) 1345–1363, doi:10.1002/aic.14732.
[10] D.C.S. Azevedo, A.E. Rodrigues, Fructose–glucose separation in a SMB pilot unit: modeling, simulation, design, and operation, AIChE J. 47 (9) (2001) 2042–2051, doi:10.1002/aic.690470915.
[11] M. Juza, M. Mazzotti, M. Morbidelli, Simulated moving-bed chromatography and its application to chirotechnology, Trends Biotechnol. 18 (3) (2000) 108–118, doi:10.1016/S0167-7799(99)01419-5.
[12] J. Strube, F. Grote, J.P. Josch, R. Ditz, Process development and design of downstream processes, Chem. Ing. Tech. 83 (7) (2011) 1044–1065, doi:10.1002/cite.201100017.
[13] J.F. Buyel, R. Fischer, Scale-down models to optimize a filter train for the downstream purification of recombinant pharmaceutical proteins produced in tobacco leaves, Biotechnol. J. 9 (3) (2014) 415–425, doi:10.1002/biot.201300369.
[14] T. Tajsoleiman, L. Mears, U. Krühne, K.V. Gernaey, S. Cornelissen, An industrial perspective on scale-down challenges using miniaturized bioreactors, Trends Biotechnol. 37 (7) (2019) 697–706, doi:10.1016/j.tibtech.2019.01.002.
[15] H.J. Subramani, A.S. Kurup, Micro-simulated moving bed (μSMB) systems: a numerical study, Chem. Eng. J. 120 (3) (2006) 169–179, doi:10.1016/j.cej.2006.04.002.
[16] J.W. Baier, R.C. Mierendorf, A.C. Grabski, A.P. Wilke, A.R. Oroskar, Valve module and methods for simulated moving bed chromatography, 2014, https://patents.google.com/patent/US8807164B2/en.
[17] S. Nagamatsu, O. Ludemann-Hombourger, J. Filou, Simulated moving bed device, 2003. https://patents.google.com/patent/US6544413B1/en.
[18] R.T. Sprague, G.P. Towler, A.R. Oroskar, Miniature actual moving bed assembly, 2005, https://patents.google.com/patent/US6979402B1/en.
[19] A.R. Oroskar, S.P. Parikh, A.A. Oroskar, K.U. Johnson, A.J. Escarcega, Valve and process for interrupted continuous flow chromatography, 2009. https://patents.google.com/patent/US7544293B2/en.
[20] M. Pedeferri, G. Zenoni, M. Mazzotti, M. Morbidelli, Experimental analysis of a chiral separation through simulated moving bed chromatography, Chem. Eng. Sci. 54 (17) (1999) 3735–3748, doi:10.1016/S0009-2509(99)00031-7.
[21] T. Kröber, M.W. Wolff, B. Hundt, A. Seidel-Morgenstern, U. Reichl, Continuous purification of influenza virus using simulated moving bed chromatography, J. Chromatogr. A 1307 (2013) 99–110, doi:10.1016/j.chroma.2013.07.081.
[22] A. Seidel-Morgenstern, L.C. Keßler, M. Kaspereit, New developments in simulated moving bed chromatography, Chem. Eng. Technol. 31 (6) (2008) 826–837, doi:10.1002/ceat.200800081.
[23] M. Mazzotti, G. Storti, M. Morbidelli, Optimal operation of simulated moving bed units for nonlinear chromatographic separations, J. Chromatogr. A (1997) 22.
[24] A. Rodrigues, Simulated Moving Bed Technology: Principles, Design and Process Applications, Butterworth-Heinemann, 2015. Google-Books-ID: qPGcBAAAQBAJ
[25] K. Hashimoto, S. Adachi, Y. Shirai, Continuous desalting of proteins with a simulated moving-bed adsorber, Agric. Biol. Chem. 52 (9) (1988) 2161–2167, doi:10.1080/00021369.1988.10869005.
[26] A.G. Rios, A.M. Ribeiro, A.E. Rodrigues, A.F.P. Ferreira, Bovine serum albumin and myoglobin separation by size exclusion SMB, J. Chromatogr. A 1628 (2020) 461431, doi:10.1016/j.chroma.2020.461431.
[27] Y. Xie, S. Mun, J. Kim, N.-H. Wang, Standing wave design and experimental validation of a tandem simulated moving bed process for insulin purification, Biotechnol. Prog. 18 (6) (2002) 1332–1344, doi:10.1021/bp025547r.
[28] Tosoh, Octave 12 Pump, 2022 https://sembabio.com/octave-12-pump-chromatography/.
[29] Sartorius, BioSMB PD, 2022 https://www.sartorius.com/en/products/process-chromatography/chromatography-systems/continuous-chromatography/biosmb-pd.
[30] K.B. Lynch, A. Chen, S. Liu, Miniaturized high-performance liquid chromatography instrumentation, Talanta 177 (2018) 94–103, doi:10.1016/j.talanta.2017.09.016.
[31] L. Li, X. Wang, Q. Pu, S. Liu, Advancement of electroosmotic pump in microflow analysis: a review, Anal. Chim. Acta 1060 (2019) 1–16, doi:10.1016/j.aca.2019.02.004.
[32] W. Zeng, S. Li, Z. Wang, Characterization of syringe-pump-driven versus pressure-driven microfluidic flows, in: 2015 International Conference on Fluid Power and Mechatronics (FPM), 2015, pp. 711–715, doi:10.1109/FPM.2015.7337207.
[33] N. Mavrogiannis, M. Ibo, X. Fu, F. Crivellari, Z. Gagnon, Microfluidics made easy: a robust low-cost constant pressure flow controller for engineers and cell biologists, Biomicrofluidics 10 (3) (2016) 034107, doi:10.1063/1.4950753. Publisher: American Institute of Physics
[34] J. Knoška, L. Adriano, S. Awel, K.R. Beyerlein, O. Yefanov, D. Oberthuer, G.E. Peña Murillo, N. Roth, I. Sarrou, P. Villanueva-Perez, M.O. Wiedorn, F. Wilde, S. Bajt, H.N. Chapman, M. Heymann, Ultracompact 3D microfluidics for time-resolved structural biology, Nat. Commun. 11 (1) (2020) 657, doi:10.1038/s41467-020-14434-6. Number: 1 Publisher: Nature Publishing Group
[35] M. Minceva, A.E. Rodrigues, Influence of the transfer line dead volume on the performance of an industrial scale simulated moving bed for p-xylene separation, Sep. Sci. Technol. 38 (7) (2003) 1463–1497, doi:10.1081/SS-120019088. Publisher: Taylor & Francis
[36] W. Jin, P.C. Wankat, Thermal operation of four-zone simulated moving beds, Ind. Eng. Chem. Res. 46 (22) (2007) 7208–7220, doi:10.1021/ie070047u. Publisher: American Chemical Society
[37] C. Migliorini, M. Mazzotti, M. Morbidelli, Simulated moving-bed units with extra-column dead volume, AIChE J. 45 (7) (1999) 1411–1421, doi:10.1002/aic.690450706.
[38] P.S. Gomes, M. Zabkova, M. Zabka, M. Minceva, A.E. Rodrigues, Separation of chiral mixtures in real SMB units: the FlexSMB-LSRE®, AIChE J. 56 (1) (2010) 125–142, doi:10.1002/aic.11962.
[39] R.P. Faria, A.E. Rodrigues, Instrumental aspects of simulated moving bed chromatography, J. Chromatogr. A 1421 (2015) 82–102, doi:10.1016/j.chroma.2015.08.045.
[40] J. Diehm, V. Hackert, M. Franzreb, Configurable 3D printed microfluidic multiport valves with axial compression, Micromachines 12 (10) (2021) 1247, doi:10.3390/mi12101247.
[41] V. Gnyawali, M. Saremi, M.C. Kolios, S.S.H. Tsai, Stable microfluidic flow focusing using hydrostatics, Biomicrofluidics 11 (3) (2017) 034104, doi:10.1063/1.4983147. Publisher: American Institute of Physics
[42] R. Bermejo, F. Gabriel Acién, M.J. Ibáñez, J.M. Fernández, E. Molina, J.M. Alvarez-Pez, Preparative purification of B-phycoerythrin from the microalga Porphyridium cruentum by expanded-bed adsorption chromatography, J. Chromatogr. B 790 (1) (2003) 317–325, doi:10.1016/S1570-0232(03)00168-5.
[43] J.G. Ziegler, N.B. Nichols, Optimum settings for automatic controllers, J. Dyn. Syst. Meas. Control 115 (2B) (1993) 220–222, doi:10.1115/1.2899060.
[44] R. Qin, C. Duan, The principle and applications of Bernoulli equation, J. Phys. Conf. Ser. 916 (2017) 012038, doi:10.1088/1742-6596/916/1/012038.
[45] A. Podgornik, Pressure drop in liquid chromatography, J. Sep. Sci. 42 (1) (2019) 72–88, doi:10.1002/jssc.201800882.
[46] G. Storti, M. Mazzotti, M. Morbidelli, S. Carrà, Robust design of binary countercurrent adsorption separation processes, AIChE J. 39 (3) (1993) 471–492, doi:10.1002/aic.690390310.
[47] H. Schmidt-Traub, M. Schulte, A. Seidel-Morgenstern, Preparative Chromatography, second ed., John Wiley & Sons, Ltd, 2012, doi:10.1002/9783527649280.
[48] S. Leweke, E. von Lieres, Chromatography analysis and design toolkit (CADET),

Comput. Chem. Eng. 113 (2018) 274–294, doi:10.1016/j.compchemeng.2018.02.025.
[49] Q.-L. He, S. Leweke, E. von Lieres, Efficient numerical simulation of simulated moving bed chromatography with a single-column solver, Comput. Chem. Eng. 111 (2018) 183–198, doi:10.1016/j.compchemeng.2017.12.022.
[50] A. Püttmann, S. Schnittert, U. Naumann, E. von Lieres, Fast and accurate parameter sensitivities for the general rate model of column liquid chromatography, Comput. Chem. Eng. 56 (2013) 46–57, doi:10.1016/j.compchemeng.2013.04.021.
[51] A. Püttmann, S. Schnittert, S. Leweke, E. von Lieres, Utilizing algorithmic differentiation to efficiently compute chromatograms and parameter sensitivities, Chem. Eng. Sci. 139 (2016) 152–162, doi:10.1016/j.ces.2015.08.050.
[52] I. of Bio-and Geosciences 1 (IBG-1) of Forschungszentrum Jülich, General rate model (GRM) – CADET. https://cadet.github.io/master/modelling/unit_operations/general_rate_model.html.
[53] S.F. Chung, C.Y. Wen, Longitudinal dispersion of liquid flowing through fixed and fluidized beds, AlChE J. 14 (6) (1968) 857–866, doi:10.1002/aic.690140608.
[54] E.J. Wilson, C.J. Geankoplis, Liquid mass transfer at very low Reynolds numbers in packed beds, Ind. Eng. Chem. Fundam. 5 (1) (1966) 9–14, doi:10.1021/i160017a002.
[55] C.N. Satterfield, C.K. Colton, W.H. Pitcher Jr., Restricted diffusion in liquids within fine pores, AlChE J. 19 (3) (1973) 628–635, doi:10.1002/aic.690190332.
[56] C. Chen, B.T. Mehl, A.S. Munshi, A.D. Townsend, D.M. Spence, R. Scott Martin, 3D-printed microfluidic devices: fabrication, advantages and limitations–a mini review, Anal. Methods 8 (31) (2016) 6005–6012, doi:10.1039/C6AY01671E. Publisher: Royal Society of Chemistry